Supporting Information: Activity and Degradation of Pt-Co and Pt-Ni Alloy Catalysts for Application in High-temperature PEM Fuel Cells

Jan Dismas Buriánek[1], Martin Prokop[1], Tomas Bystron[1], Martin Veselý[2], Lukáš Koláčný[2], Bruna Ferreira Gomes[3], Carlos Manuel Silva Lobo[3], Matija Gatalo[4,5], Luka Pavko[4,5], Nejc Hodnik[4], Martin Paidar[1], Christina Roth[3], Miran Gaberscek[4], Karel Bouzek[1]*
Department of Inorganic Technology, University of Chemistry and Technology Prague, Technická 5, 166 28, Praha, Czech Republic
[2]Department of Organic Technology, University of Chemistry and Technology Prague, Technická 5, 166 28 Praha, Czech Republic
[3]Electrochemical Process Engineering, University of Bayreuth, Universitätsstraße 30, Bayreuth, 95447, Germany
[4]Department of Materials Chemistry, National Institute of Chemistry, Hajdrihova 19, p.p. 660, SI-1001 Ljubljana, Slovenija
[5]ReCatalyst, Hajdrihova 19, 1001 Ljubljana, Slovenia
**Corresponding author*

Keywords: High-temperature polymer electrolyte membrane fuel cells, alloy catalysts, oxygen reduction reaction, rotating rod disk electrode, phosphoric acid, dealloying

Contents

1 Experimental

S1.1 Graphene oxide synthesis

Graphene oxide (GO) was synthesised using a modified Hummer's method reported previously [1]. In a 5 dm^3 beaker, 1 dm^3 of 96 wt.% H_2SO_4 (Suprapure, Merck, Germany) was mixed with 110 cm^3 of 85 wt.% H_3PO_4. Graphite (Imerys, Switzeland) was added, followed by $KMnO_4$ (99.9%, Carlo Erba) increments every 24 h, totalling 5 wt. eq. (a total mass of five times the mass of graphite). After two days of stirring, the reaction was quenched with ice and 30 wt.% H_2O_2 until coloured changed from purple to yellow. The resulting GO settled overnight, and the supernatant was replaced with ultrapure water. Additional washing steps included dispersion in 5 wt.% HCl, centrifugation, and re-dispersion in ultrapure water with multiple cycles. The final GO suspension was treated with a homogeniser for 1 h in an ice bath.

S1.2 Pt-Co(Ni) catalyst synthesis

The synthesis involved producing Ketjenblack (KB) and reduced graphene oxide (rGO) supported Co(Ni)/KB composite materials using the pulse combustion reactor reported previously [2]. For Co/KB, 75.4 g of $Co(AcO)_2{\cdot}4H_2O$ (99.9 wt.%, Sigma Aldrich) and 30 g of KB EC300J (Nouryon, Netherlands) were mixed in 1 dm^3 of ultrapure water. Similarly, for Ni/KB synthesis, 75.4 g of $Ni(AcO)_2{\cdot}4H_2O$ (99.9 wt.% Sigma Aldrich) were utilised. In the case of Co/rGO, 25.0 g of $Co(AcO)_2{\cdot}4H_2O$ was dissolved in 1 dm^3 of ~14 g GO dm^{-3} ultrapure water suspension. These precursors were mixed vigorously using a homogeniser for 10 min before introduction to the pulse combustion reactor. In summary, materials were synthesised in a reactor utilising a specialised combustor. The combustor receives air through a valve powered by a blower, and the airflow is measured with a thermal mass flow meter. The fuel, C_3H_8, is regulated by another meter and controller. The appropriate ratio of fuel to air is set by adjusting the blower speed or fuel flow. Additionally, C_3H_8 can be mixed with N_2 to control pressure fluctuations in the reactor. These fluctuations impact temperature and gas composition, leading to more efficient fuel combustion with reduced O_2 amount. The combustor features a secondary inlet for C_2H_2, injected to enhance the reductive atmosphere. A T-section enables the spraying of precursors into the hot zone of the reactor where the precursors are introduced to the flue gas where nanoparticles form on KB or rGO support. Co(Ni)/KB composites are collected with an electrostatic filter. The intermetallic Pt-alloy electrocatalysts, were prepared by depositing Pt nanoparticles on the prepared Co/KB, Ni/KB or Co/rGO composites through the double passivation galvanic displacement method reported previously [3]. The composites with

deposited Pt nanoparticles were further thermally annealed for intermetallic crystal phase formation in Ar atmosphere at 700 °C for 5 h. Finally, all the prepared catalysts, including Pt-Co/KB, Pt-Ni/KB and Pt-Co/rGO, underwent chemical activation, following established procedures [4] which involve acid treatment followed by multiple washing cycles.

S1.3 In-situ XAS cell

The core of the cell consisted of a PTFE block (5 cm × 6 cm × 2 cm) with a milled cavity (2 cm × 2.5 cm × 0.4 cm, corresponding to 2 cm^3). A 2 cm × 2 cm square was cut from a GDE and affixed to the cavity from the inside using Kapton tape (80 μm), such that the catalyst layer of GDE faced outward and was additionally sealed with Kapton tape.

Duralumin plates, each 1 cm thick, were mounted on both sides of the PTFE block. The rear plate was planar, while the front plate featured a conical hole (2 to 3 cm in diameter), positioned above the GDE to allow X-ray transmission through the catalyst layer. A PEEK spacer (Spectra/Mesh, Spectra Laboratories) was inserted between the PTFE block and the front duralumin plate to ensure proper sealing.

The assembly was finalised with insulating components: a rear layer made from 1 cm thick inorganic aluminosilicate fire-resistant composite, and two 0.5 cm thick PTFE plates on the outermost sides. These outer PTFE plates extended vertically by 1 cm beyond the core cell body and served as support legs. The duralumin plates were equipped with two 35 W cylindrical heating cartridges (diameter 2.5 mm, length 30 mm, Omega, USA). Temperature was monitored via a thermocouple (5SRTC, Omega, USA) inserted into the PTFE block and regulated by a home-built PID temperature controller.

At the beginning of each experiment, 1.6 cm^3 of 95 wt.% H_3PO_4 solution (prepared from crystalline H_3PO_4 and demineralised water) was pipetted into the pre-heated cell. The cell was heated to 100, 140, 160, or 180 °C. A fresh GDE sample was used at each temperature and absorption edge to avoid signal degradation. XAS spectra were acquired at the Pt L_3-edge and the Co and Ni K-edges. . Each in-situ measurement lasted 4 h during which XAS spectra (each 3 min long) were continuously recorded. The average time delay between acid injection into the pre-heated cell and end of acquisition of the first XAS spectrum was around 12 min. Exact delay times for individual experiment are reported in the following sections. Each individual scan required 3 min for completion. The measurements were performed in fluorescence (PIPS detector) mode. The corresponding metallic foils were measured simultaneously with the samples to align the energy. The same software and the same data processing as in the case of ex-situ samples were used.

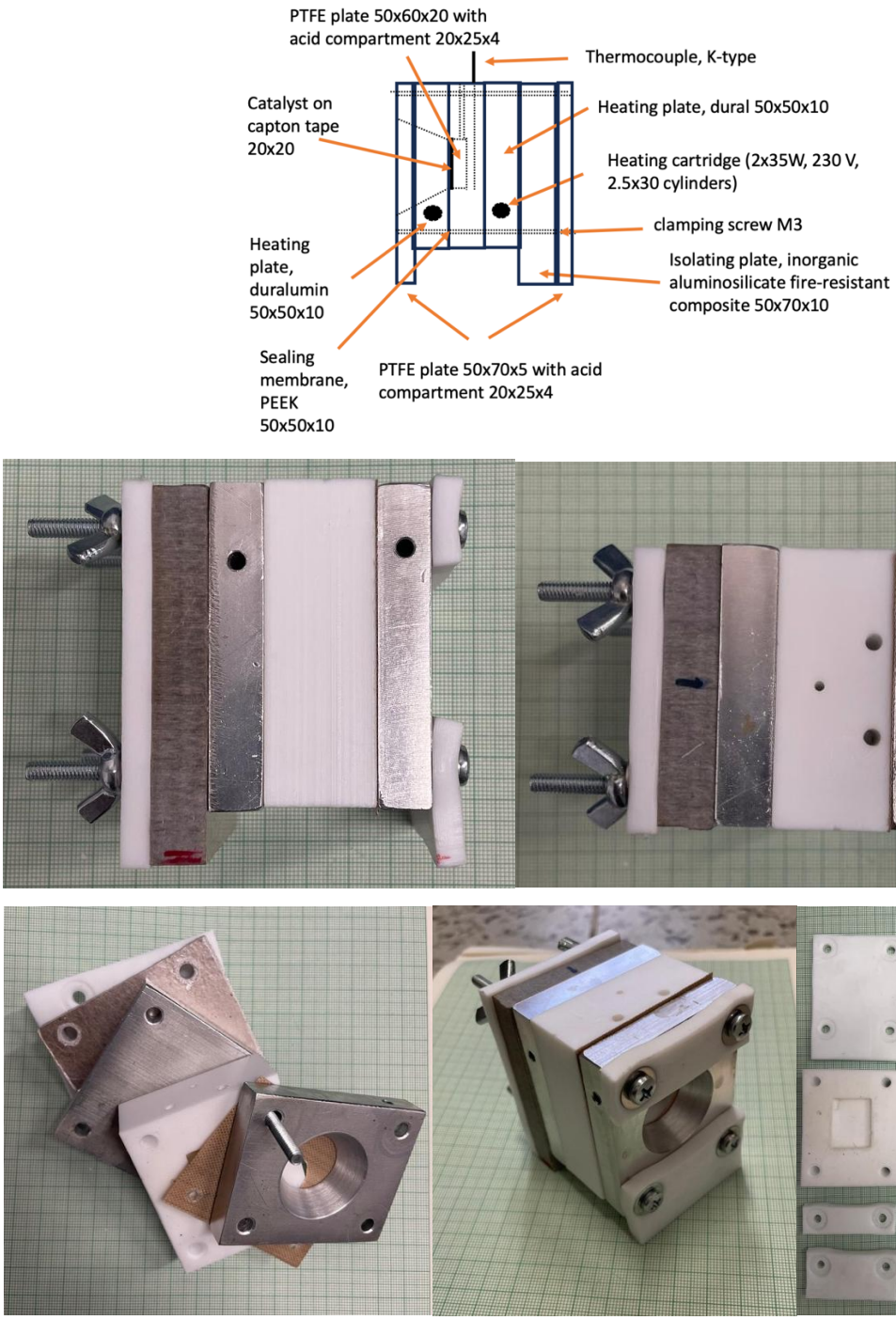

Figure S1.1*: In-situ XAS measuring cell. All dimension in mm. Photographs were taken on millimeter paper to provide a scale reference*

2 ORR activity of the catalysts in aqueous $HClO_4$ at 25 ºC

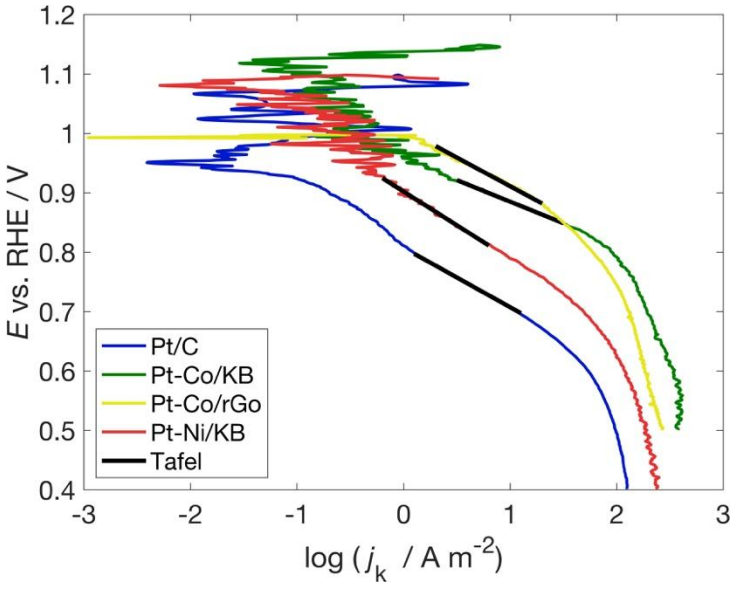

Figure S2.1*: Tafel slopes, K-L, kinetic currents of pristine catalysts calculated from various revolution rates (400-900-1600-2500 rpm); RDE electrode, 25 °C, 10* μg_{metals} cm^{-2} *of catalyst, 0.5 mol* dm^{-3} $HClO_4$*, 10 mV* s^{-1}*, corrected for background currents and uncompensated resistance, Tafel slope evaluated in high overpotential region*

***Table S2.1**: ORR kinetic parameters of H_3PO_4 leached catalysts determined in 0.1 mol dm^{-3} $HClO_4$ at 25 °C. LSV, 1600 rpm, 20 mV s^{-1}, corrected for background currents and uncompensated resistance, use of corresponding $E_{ORR,l,T}$, thin film on GC RRE (10 μg_{metals} cm^{-2} of catalyst after leaching in 97.6 wt.% H_3PO_4 at 180 °C for 0-72 h)*

Catalyst type	Degradation time / h	Tafel slope / mV dec^{-1}	$ESCA_{CO}$ / cm^2 mg^{-1}	j_{ex} / mA m^{-2}
Pt/C	Pristine	82.0 ± 1.3	50.0 ± 3.6	6.7 ± 1.9
	1	98 ± 2	36.7 ± 1.1	37.8 ± 4.0
	3	100 ± 7	40.3 ± 6.0	30.6 ± 4.9
	8	93 ± 2	40.9 ± 4.3	16.6 ± 1.0
	24	96 ± 1	32.4 ± 2.0	23.7 ± 4.0
	72	88 ± 1	28.5 ± 1.5	8.0 ± 0.3
Pt-Co/KB	Pristine	60.6 ± 0.5	92.7 ± 8.7	30.8 ± 2.4
	1	104 ± 3	89.1 ± 1.1	26.9 ± 21.4
	3	105 ± 2	57.4 ± 6.5	45.5 ± 6.1
	8	100 ± 2	76.5 ± 5.7	37.2 ± 13.0
	24	105 ± 5	72.3 ± 0.6	50.6 ± 13.5
	72	93 ± 1	56.8 ± 1.0	15.6 ± 0.9
Pt-Co/rGO	Pristine	85.7 ± 2.9	113.0 ± 16.3	68.0 ± 0.1
	1	108 ± 2	81.0 ± 6.9	31.6 ± 14.3
	3	113 ± 4	68.3 ± 4.5	60.0 ± 6.2
	8	93 ± 1	74.0 ± 2.5	21.8 ± 1.6
	24	114 ± 5	53.1 ± 1.4	65.0 ± 18.3
	72	100 ± 3	56.5 ± 0.8	22.0 ± 4.5
Pt-Ni/KB	Pristine	68.0 ± 3.5	64.0 ± 4.2	6.9 ± 2.9
	1	90 ± 2	53.5 ± 1.8	27.4 ± 7.7
	3	94 ± 1	57.6 ± 4.5	23.6 ± 7.2
	8	100 ± 6	54.3 ± 1.6	30.5 ± 14.7
	24	102 ± 4	61.6 ± 0.7	60.1 ± 24.4
	72	90 ± 1	51.5 ± 0.3	16.3 ± 0.4

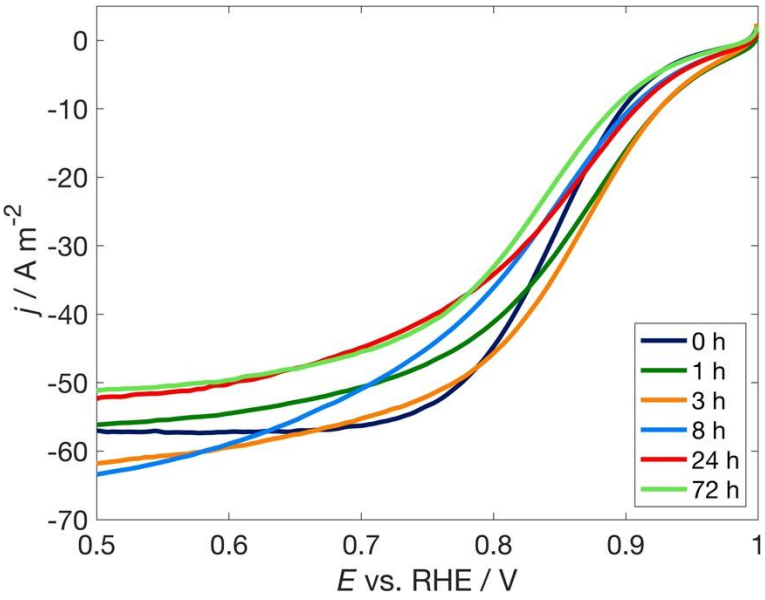

***Figure S2.2**: ORR kinetic parameters of H_3PO_4 leached catalyst determined in 0.1 mol dm^{-3} $HClO_4$ at 25 °C. LSV, 1600 rpm, 20 mV s^{-1}, corrected for background currents and uncompensated resistance, use of corresponding $E_{ORR,l,T}$, thin film on GC RRE (10 μg_{metals} cm^{-2} of Pt/C catalyst after leaching in 97.6 wt.% H_3PO_4 at 180 °C for 0-72 h)*

3 Leaching of the catalyst powders in concentrated H_3PO_4 at 180 °C

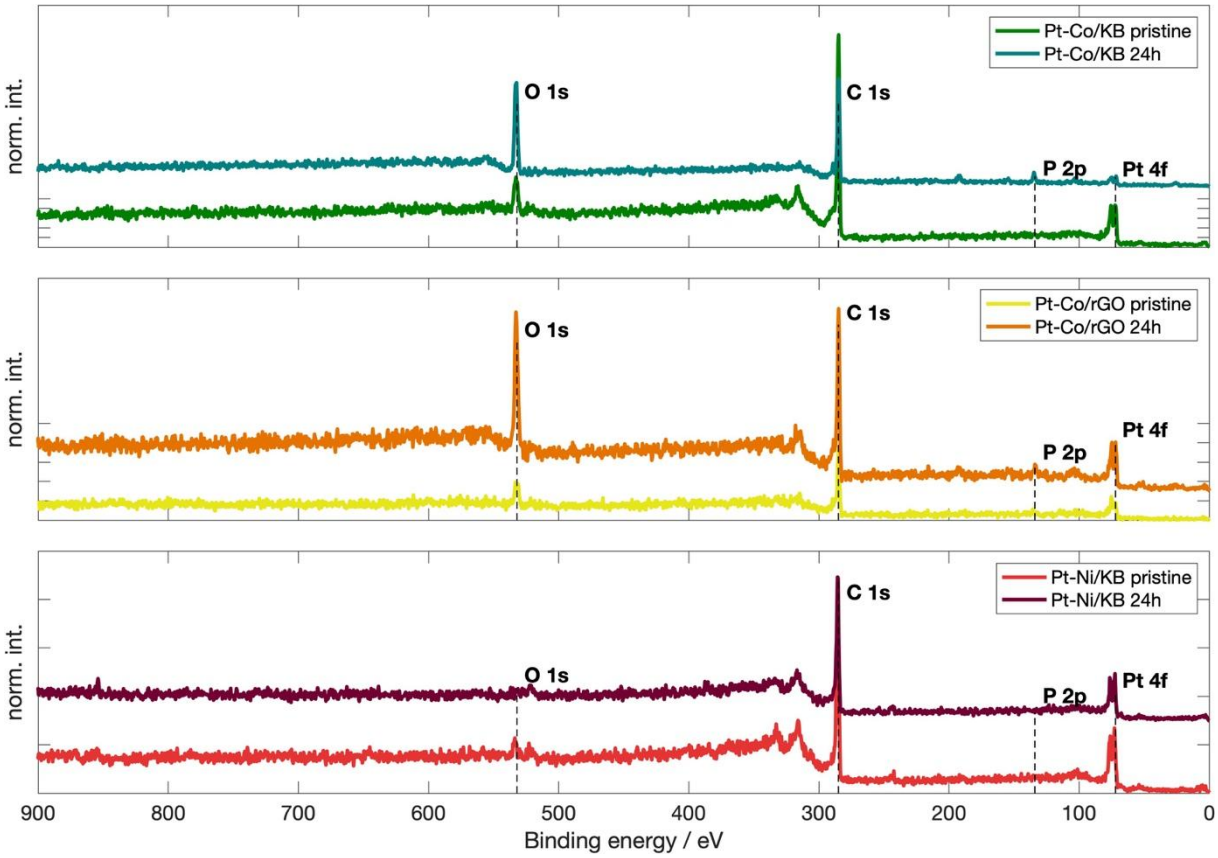

***Figure S3.1**: Survey X-ray photoelectron spectra of the catalyst samples before and after leaching in 97.6 wt.% H_3PO_4 at 180 °C for 0, 1, 3, 8, 24 and 72 h*

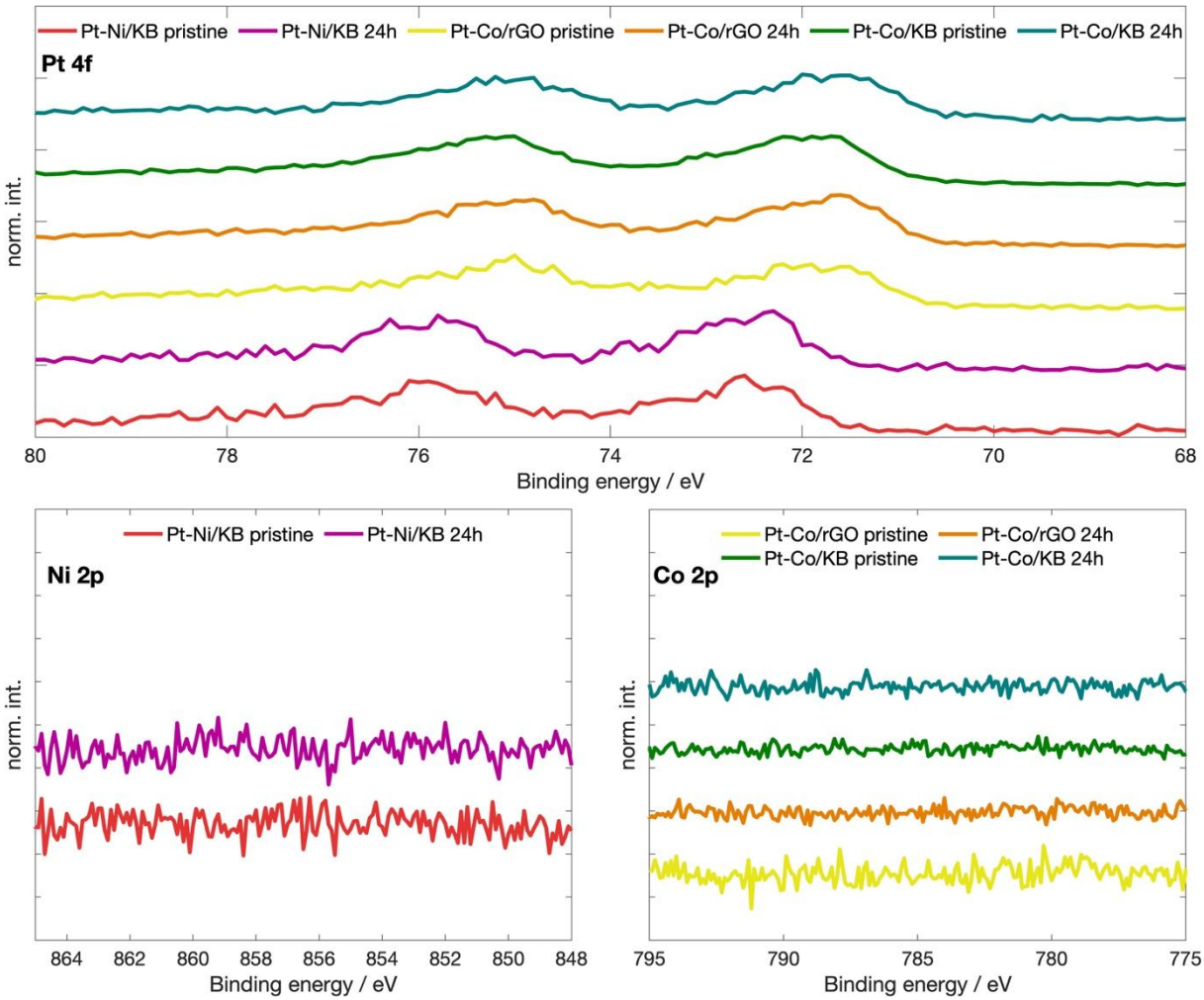

***Figure S3.2**: High-resolution X-ray photoelectron spectra of the catalyst samples before and after leaching in 97.6 wt.% H_3PO_4 at 180 °C for 0, 1, 3, 8, 24 and 72 h*

***Table S3.1:** Weight ratio of Pt to non-Pt metal ($\rho_{Pt/X,XRF}$) of the catalyst samples before and after leaching in 97.6 wt.% H_3PO_4 at 180 °C for 0, 1, 3, 8, 24 and 72 h, XRF*

Degradation time / h	Pt-Co/KB	Pt-Co/rGO	Pt-Ni/KB
0	14.5 ± 0.2	8.1 ± 0.1	5.3 ± 0.02
1	22.1 ± 0.4	15.7 ± 0.2	6.4 ± 0.03
3	20.6 ± 0.5	16.6 ± 0.2	6.4 ± 0.03
8	23.5 ± 0.5	13.1 ± 0.2	6.4 ± 0.04
24	27.6 ± 0.6	13.8 ± 0.2	6.5 ± 0.03
72	36.3 ± 0.8	18.3 ± 0.2	6.4 ± 0.05

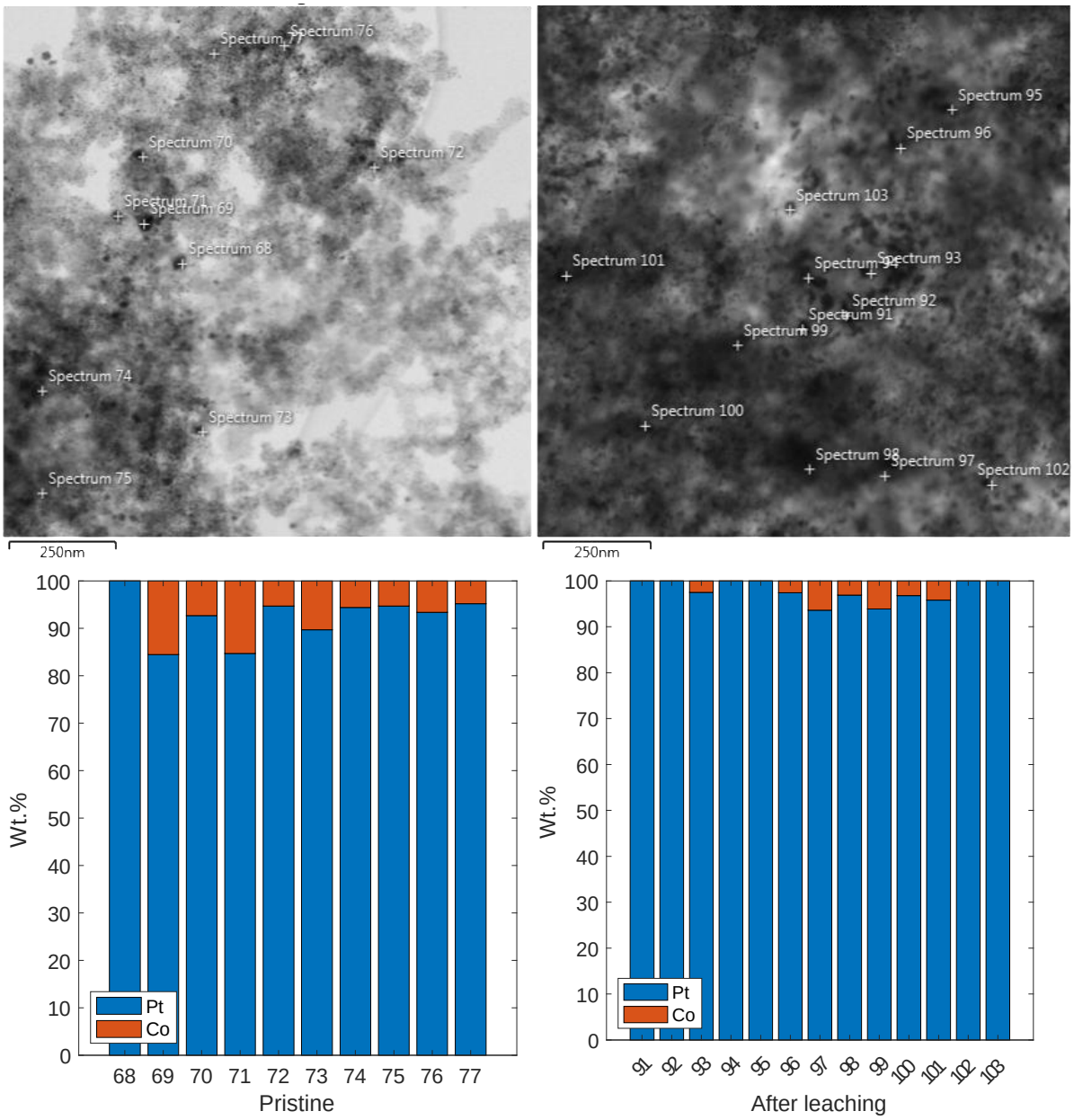

***Figure S3.3**: Distribution of Pt and Co mass fraction in multiple alloy particles, TEM/EDS spot analysis, Pt-Co/KB catalyst, pristine and after leaching in 97.6 wt.% H_3PO_4 at 180 °C for 24 h, indication of specific particles on the x-axis*

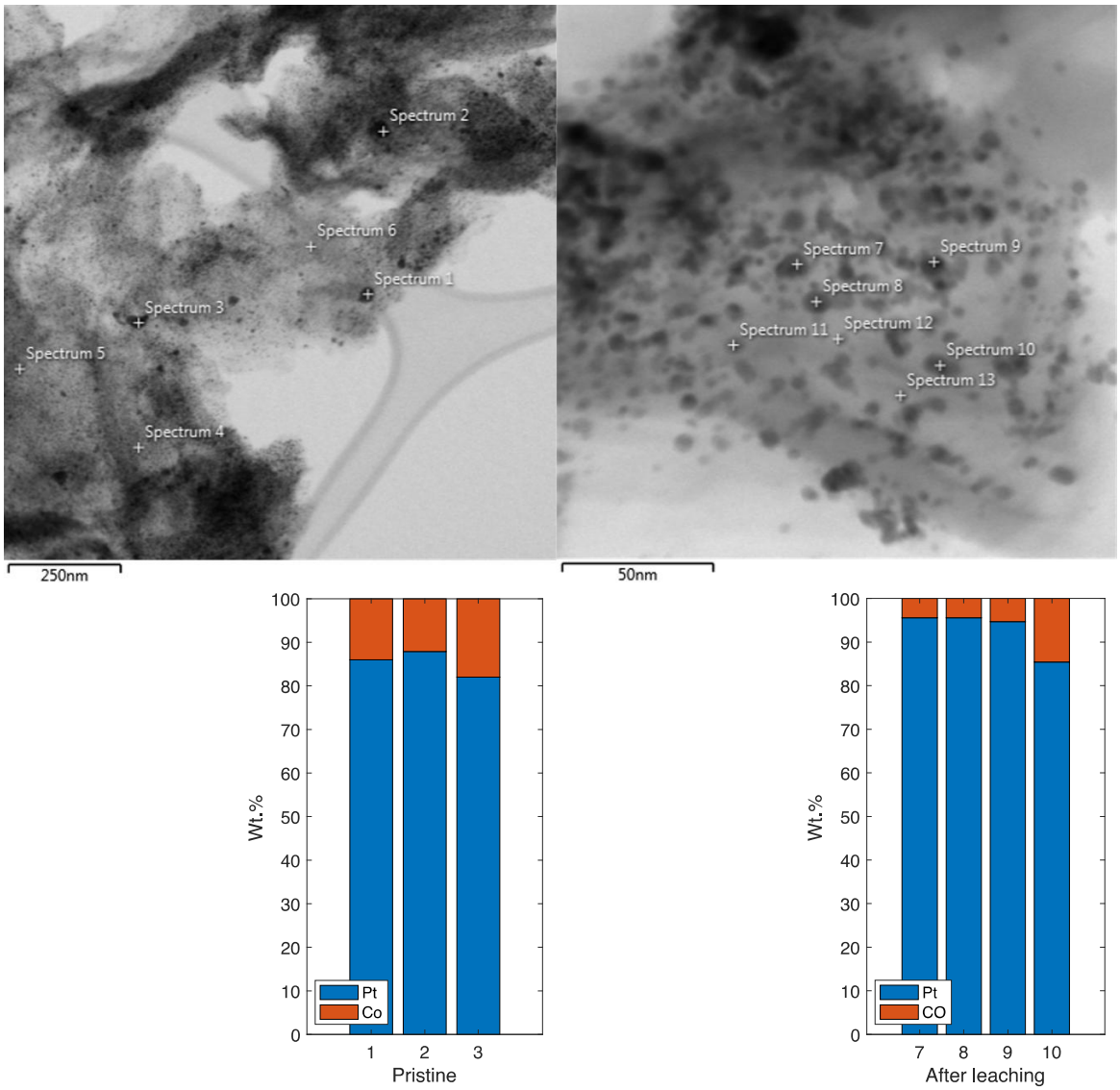

***Figure S3.4**: Distribution of Pt and Co mass fraction in multiple alloy particles, TEM/EDS spot analysis, Pt-Co/rGO catalyst, pristine and after leaching in 97.6 wt.% H_3PO_4 at 180 °C for 24 h, indication of specific particles on the x-axis*

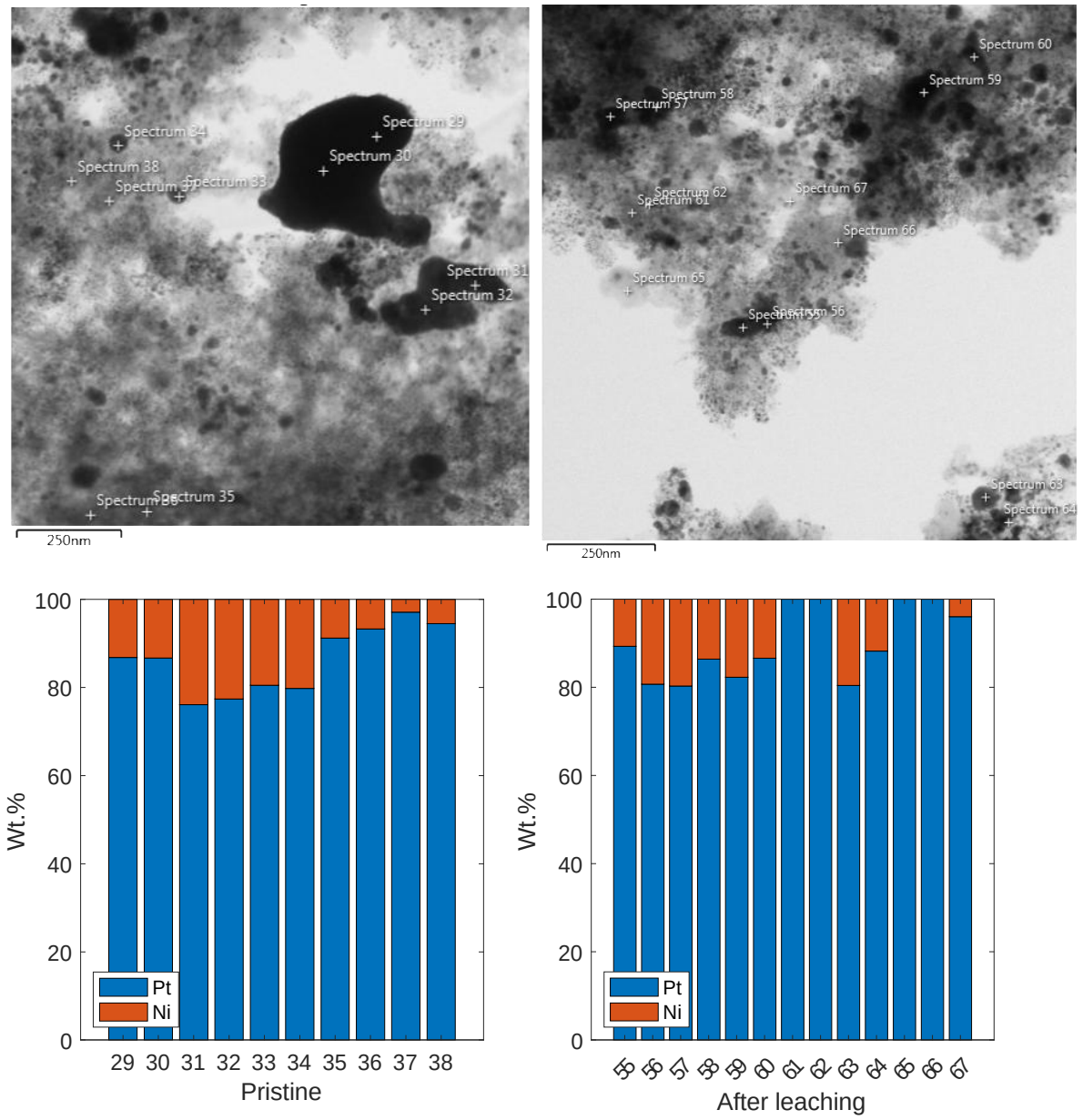

***Figure S3.5**: Distribution of Pt and Ni mass fraction in multiple alloy particles, TEM/EDS spot analysis, Pt-Ni/KB catalyst, pristine and after leaching in 97.6 wt.% H_3PO_4 at 180 °C for 24 h, indication of specific particles on the x-axis*

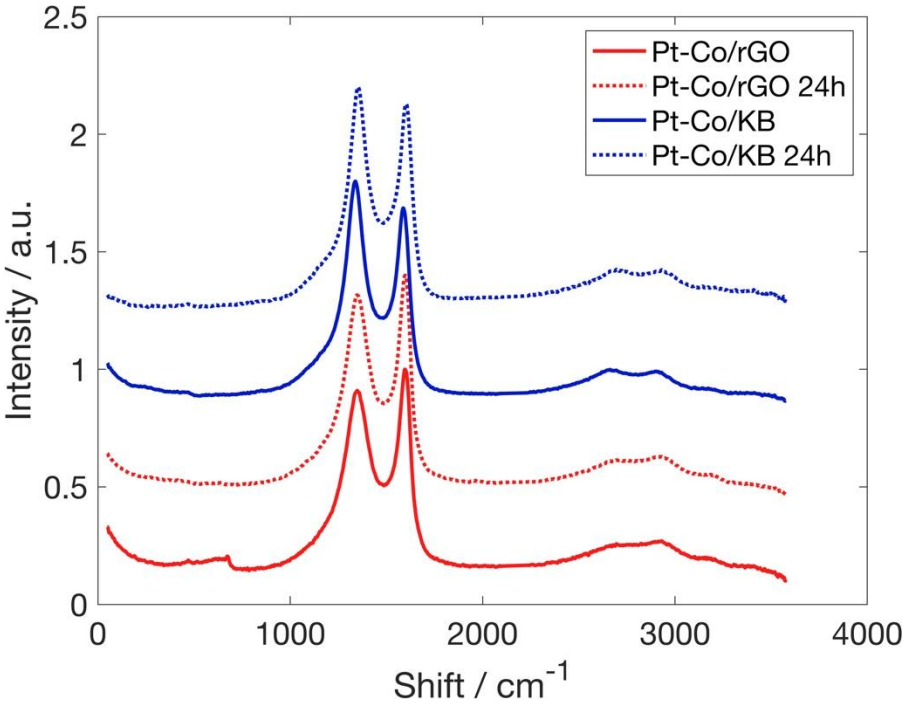

***Figure S3.6**: Raman spectra of catalysts before and after leaching in 97.6 wt.% H_3PO_4 at 180 °C for 24 h*

***Table S3.2:** Crystallite size interpreted from Pt(111) reflection of the catalyst samples before and after leaching in 97.6 wt.% H_3PO_4 at 180 °C for 1, 3, 8, 24 and 72 h, XRD, triplicate measurements were taken only at time 0 h and 24 h, the other times are represented by one sample only*

Degradation time / h	Pt/C	Pt-Co/KB	Pt-Co/rGO
0	2.70 ± 0.04	3.15 ± 0.12	3.10 ± 0.02
1	4.5	4.0	3.4
3	4.8	4.3	3.3
8	5.2	4.7	3.2
24	5.70 ± 0.89	5.08 ± 0.10	3.45 ± 0.07
72	6.3	5.3	3.5

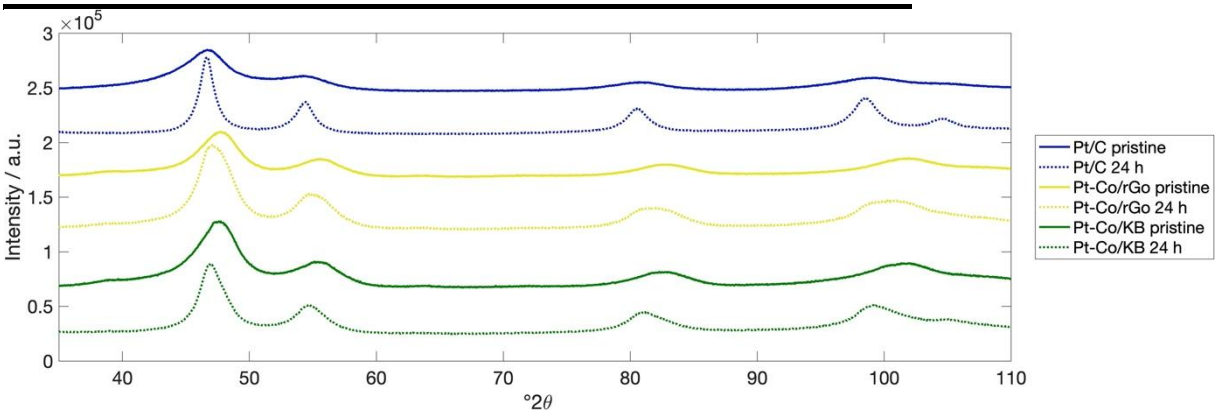

***Figure S3.7**: XRD patterns of catalysts before and after leaching in 97.6 wt.% H_3PO_4 at 180 °C for 24 h*

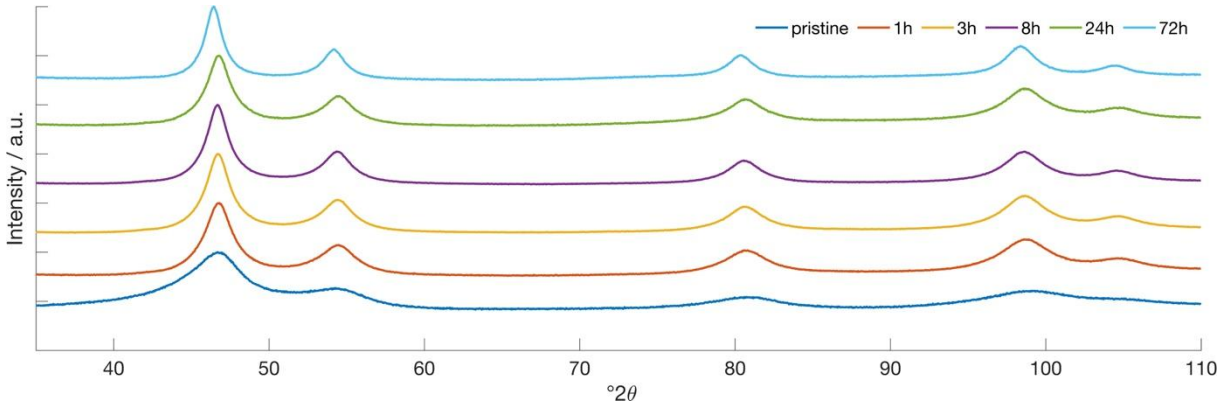

***Figure S3.8**: XRD patterns of Pt/C before and after leaching in 97.6 wt.% H_3PO_4 at 180 °C*

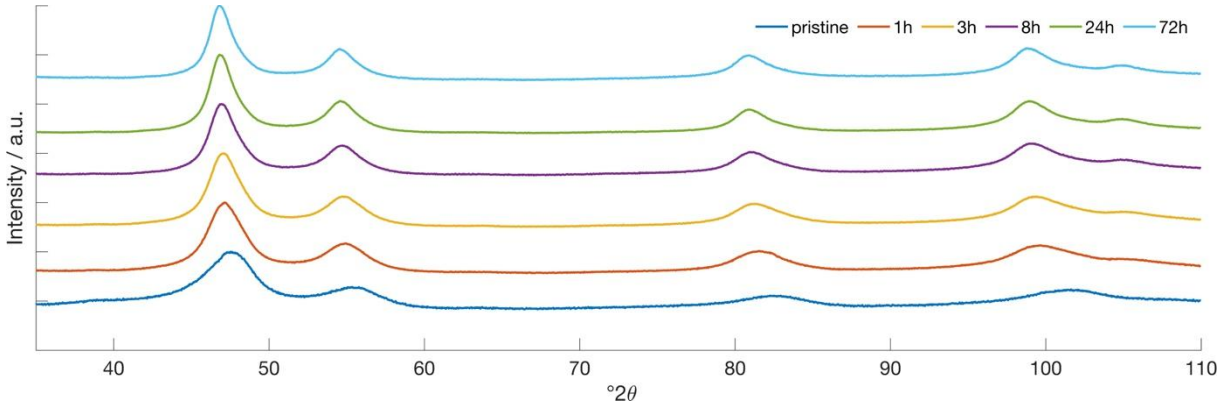

***Figure S3.9**: XRD patterns of Pt-Co/KB before and after leaching in 97.6 wt.% H_3PO_4 at 180 °C*

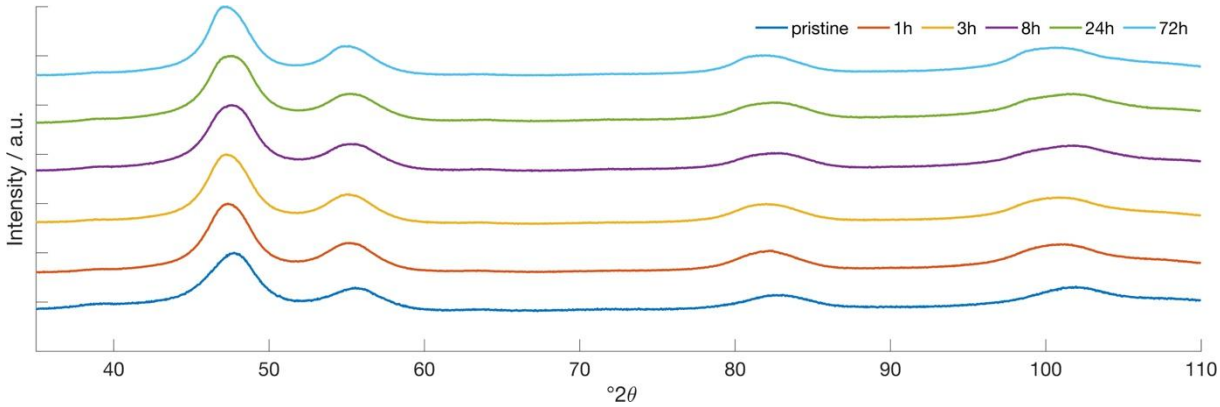

***Figure S3.10**: XRD patterns of Pt-Co/rGO before and after leaching in 97.6 wt.% H_3PO_4 at 180 °C*

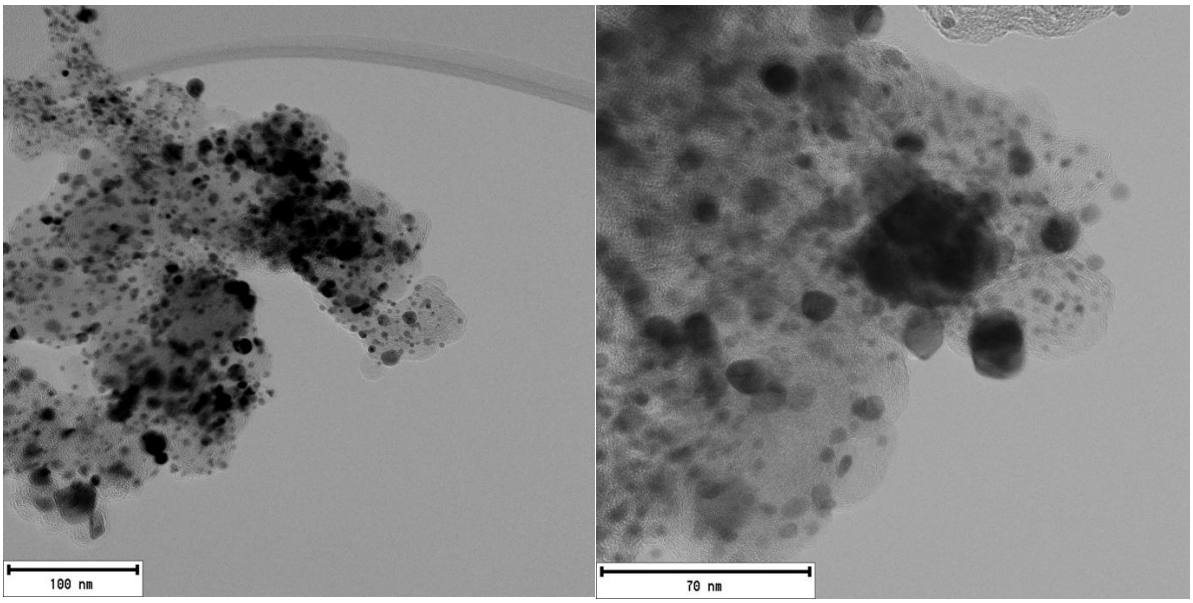

Pt-Ni/KB – pristine Pt-Ni/KB – after leaching, 24 h

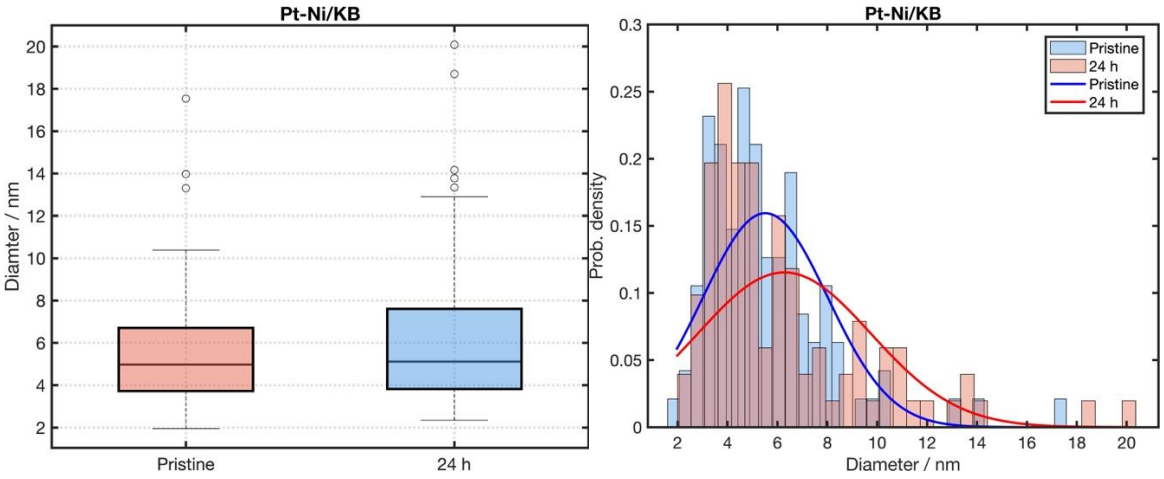

Figure S3.11*: TEM distribution size analysis of Pt-Ni/KB before and after leaching in 97.6 wt.% H_3PO_4 at 180 °C, two-sample t-test showed that the difference between the mean particle sizes was not statistically significant (p = 0.079)*

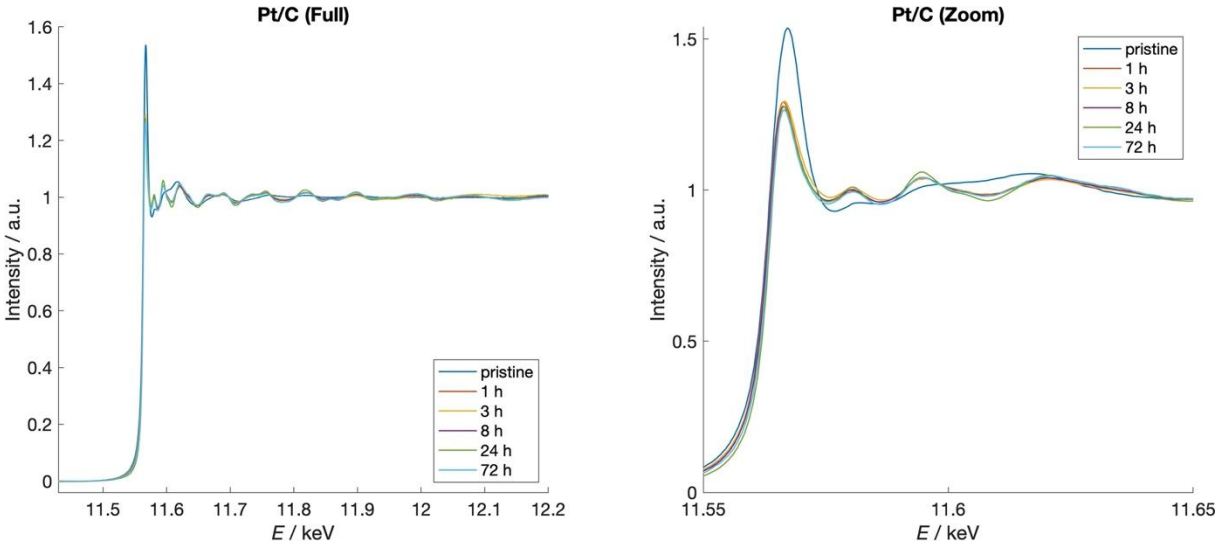

***Figure S3.12**: XAS spectra of Pt/C before and after leaching in 97.6 wt.% H_3PO_4 at 180 °C, Pt-edge*

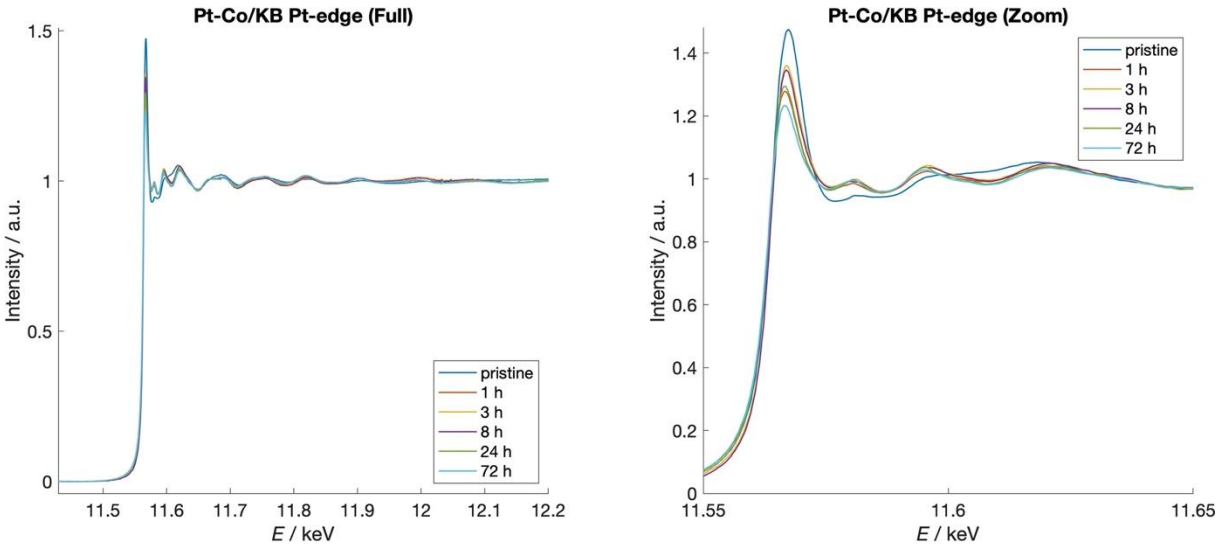

***Figure S3.13**: XAS spectra of Pt-Co/KB before and after leaching in 97.6 wt.% H_3PO_4 at 180 °C, Pt-edge*

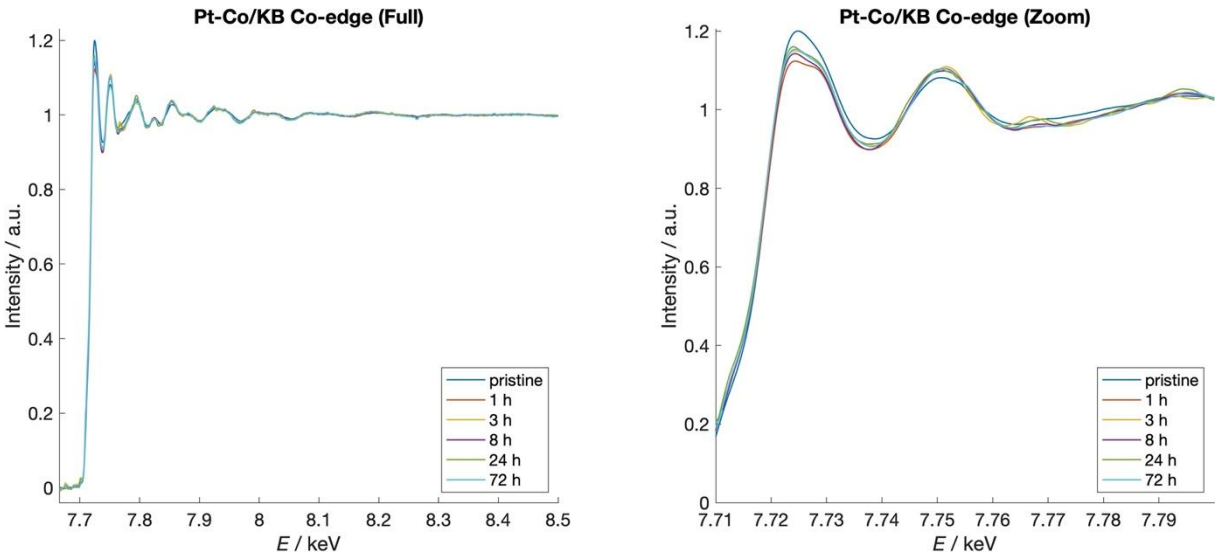

***Figure S3.14**: XAS spectra of Pt-Co/KB before and after leaching in 97.6 wt.% H_3PO_4 at 180 °C, Co-edge*

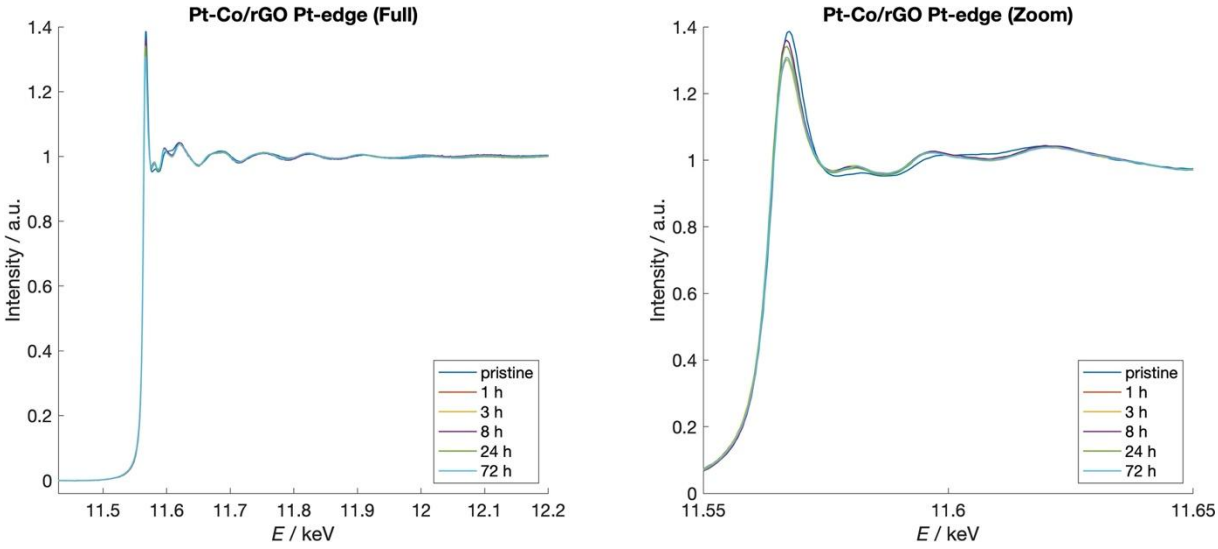

***Figure S3.15**: XAS spectra of Pt-Co/rGO before and after leaching in 97.6 wt.% H_3PO_4 at 180 °C, Pt-edge*

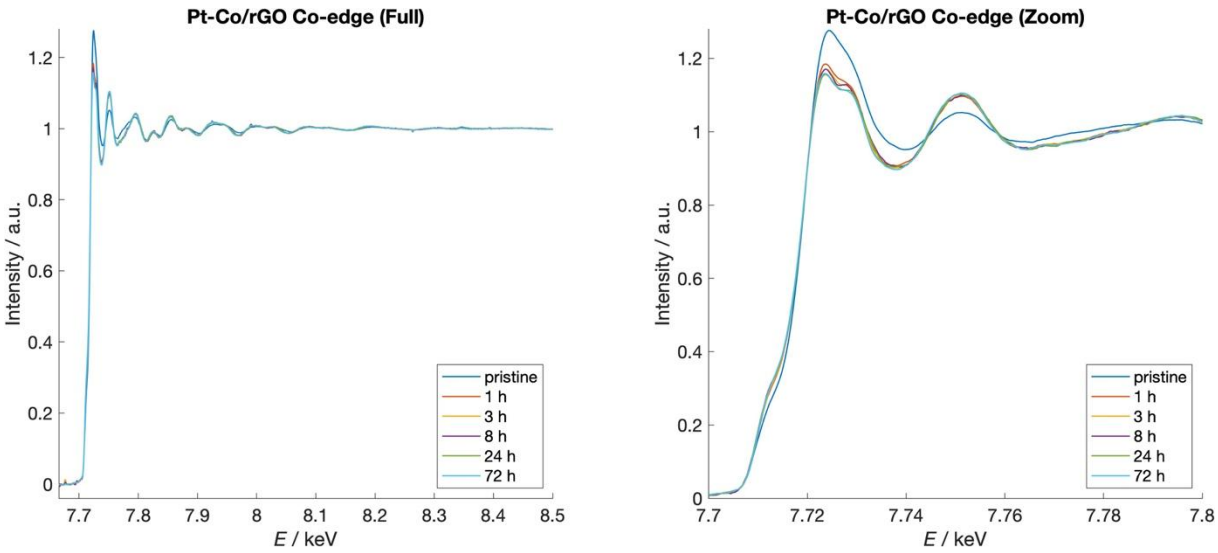

***Figure S3.16**: XAS spectra of Pt-Co/rGO before and after leaching in 97.6 wt.% H_3PO_4 at 180 °C, Co-edge*

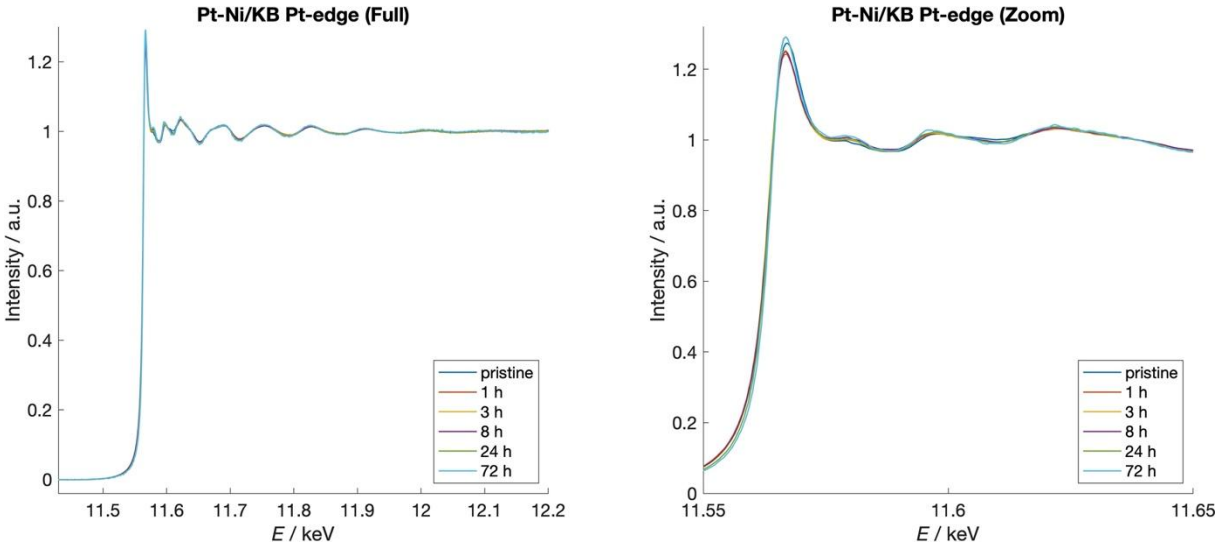

***Figure S3.17**: XAS spectra of Pt-Ni/KB before and after leaching in 97.6 wt.% H_3PO_4 at 180 °C, Pt-edge*

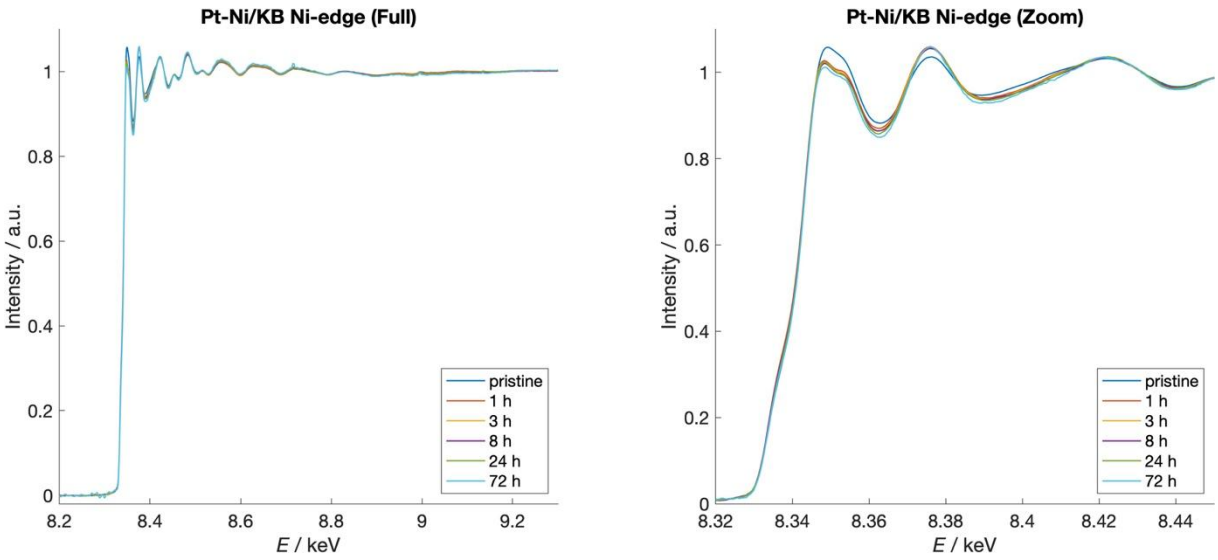

***Figure S3.18**: XAS spectra of Pt-Ni/KB before and after leaching in 97.6 wt.% H_3PO_4 at 180 °C, Ni-edge*

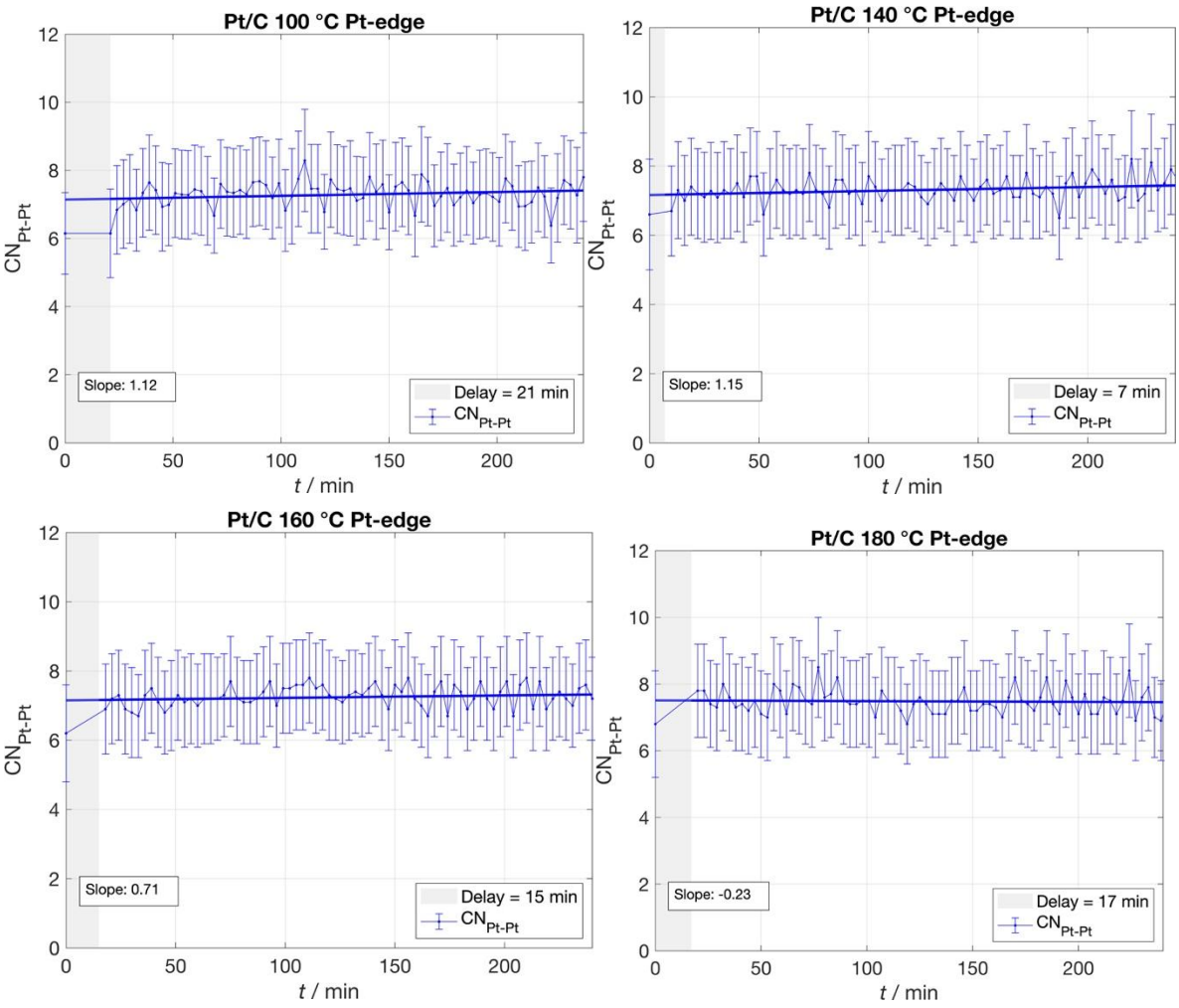

***Figure S3.19**: coordination number Pt-Pt of Pt/C, in-situ XAS in 95 wt.% H_3PO_4, GDE 1 mg_{metals} cm^{-2}, error bars of EXAFS fit (not between replicates)*

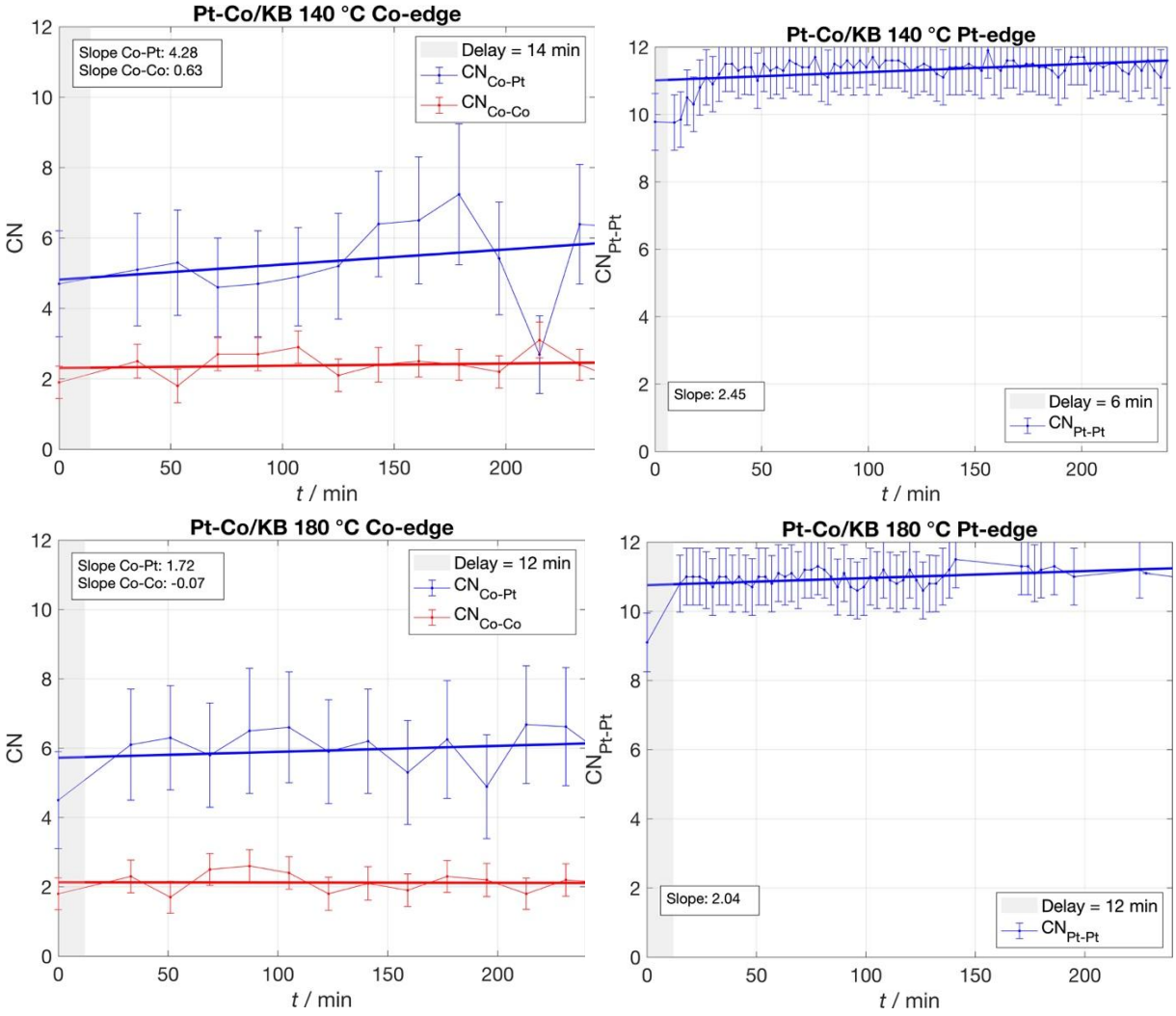

***Figure S3.20**: coordination numbers of Pt-Co/KB, in-situ XAS in 95 wt.% H_3PO_4, GDE 1 mg_{metals} cm^{-2}, Co edge 7 point average, error bars of EXAFS fit (not between replicates)*

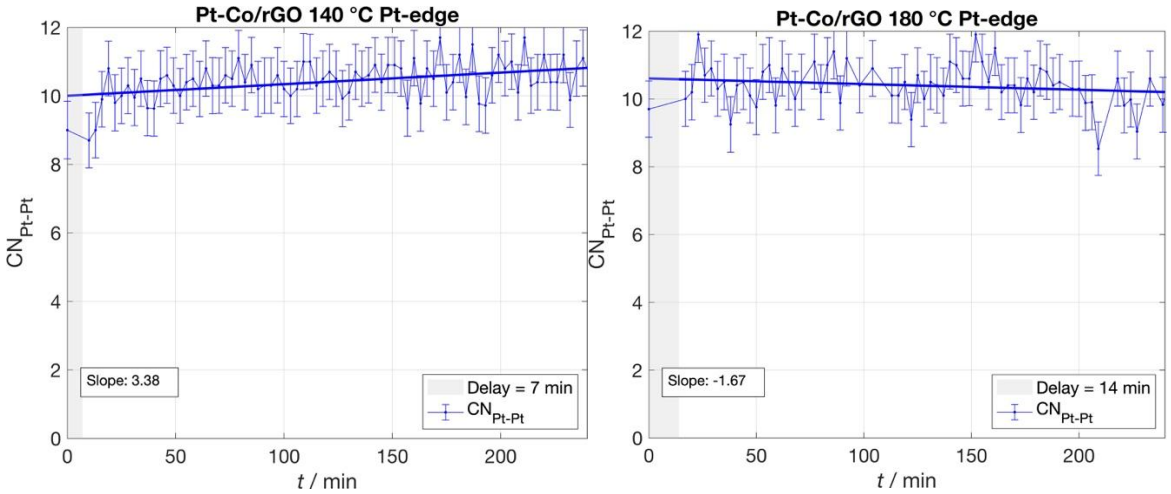

***Figure S3.21**: coordination numbers of Pt-Co/rGO, in-situ XAS in 95 wt.% H_3PO_4, GDE 1 mg_{metals} cm^{-2} (for the in situ measurements of the Pt-Co/rGO, EXAFS fitting at the Co K-edge was not feasible due to the poor signal quality. This limitation is likely related to the low concentration of Co in the alloy combined with the inherently lower data quality of rapid in situ acquisitions (3 min per scan). Moreover, the alloy undergoes compositional changes during dissolution under these experimental conditions, further reducing the signal-to-noise ratio and preventing a reliable fit of the Co K-edge), error bars of EXAFS fit (not between replicates)*

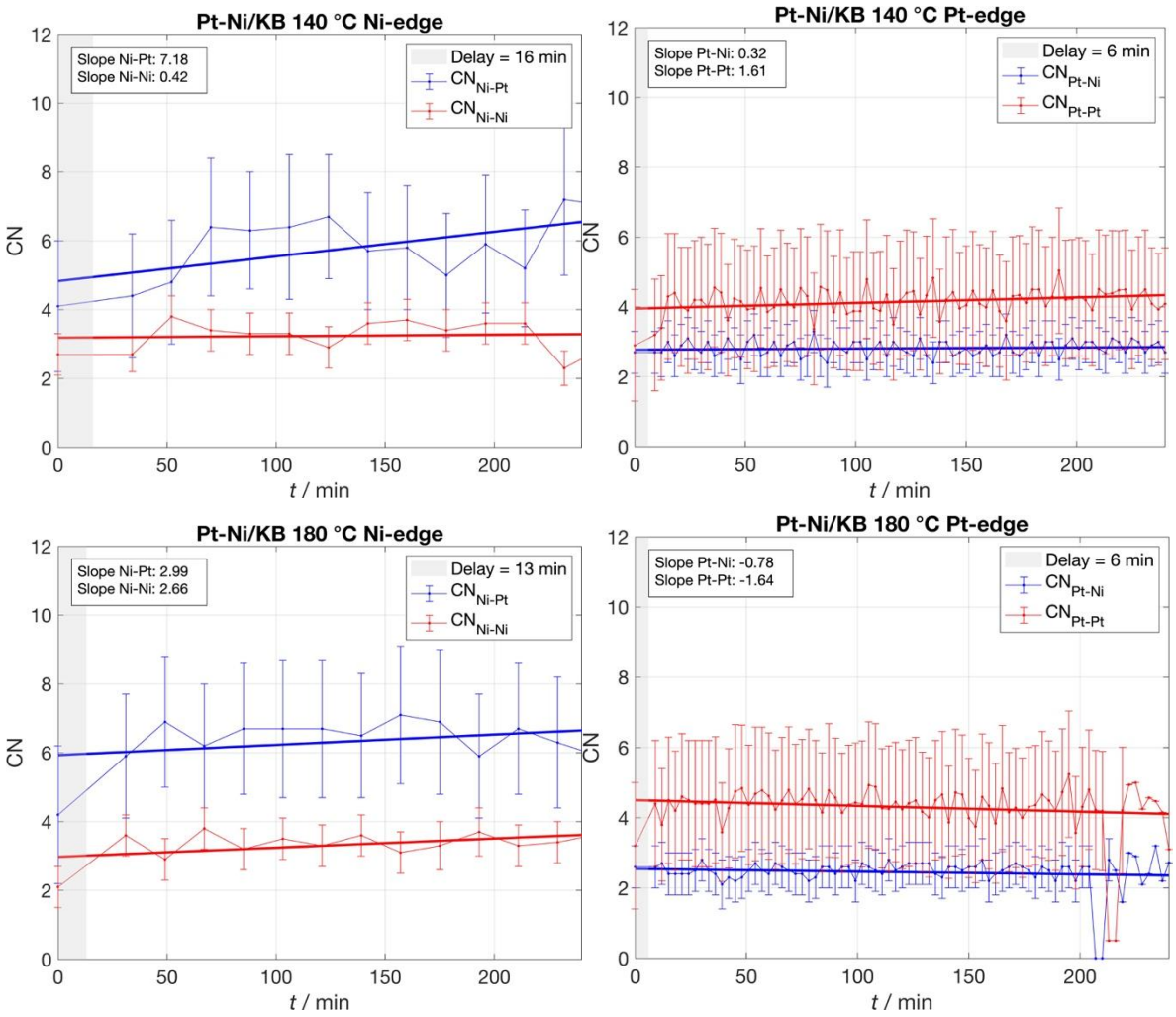

***Figure S3.22**: coordination numbers of Pt-Ni/KB, in-situ XAS in 95 wt.% H_3PO_4, GDE 1 mg_{metals} cm^{-2}, Ni-edge 7 point average, error bars of EXAFS fit (not between replicates)*

***Table S3.3:** Crystallite size interpreted from Pt(111) reflection of the catalyst samples, pristine and post-mortem XAS in 95 wt.% H_3PO_4 at various temperature, after ~4 h (specificized in table), XRD, GDE 1 mg_{metals} cm^{-2}*

Catalyst type	Degradation temperature / °C	Degradation time / min	Pt (1 1 1) / nm
Pt/C	Pristine (GDE)	–	3.8
	100	261 (4 h 21 min)	3.3

	140	247 (4 h 7 min)	3.6
	160	255 (4 h 15 min)	3.9
	180	257 (4 h 17 min)	4.2
Pt-Co/KB	Pristine (GDE)	–	4.0
	140	246 (4 h 6 min)	3.6
	180	252 (4 h 12 min)	3.8
Pt-Co/rGO	Pristine (GDE)	–	4.8
	140	247 (4 h 7 min)	3.2 (101)
	180	254 (4 h 14 min)	3.4 (101)

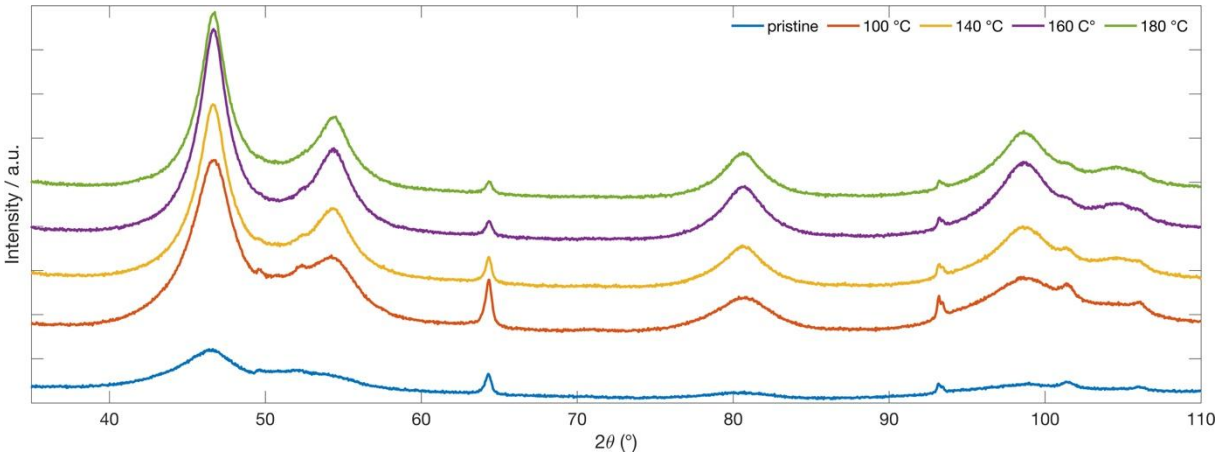

***Figure S3.23**: XRD patterns of Pt/C, pristine and post-mortem XAS in 95 wt.% H_3PO_4 at various temperature, after ~4 h (specificized in **Table S3.3**), XRD, GDE 1 mg_{metals} cm^{-2}*

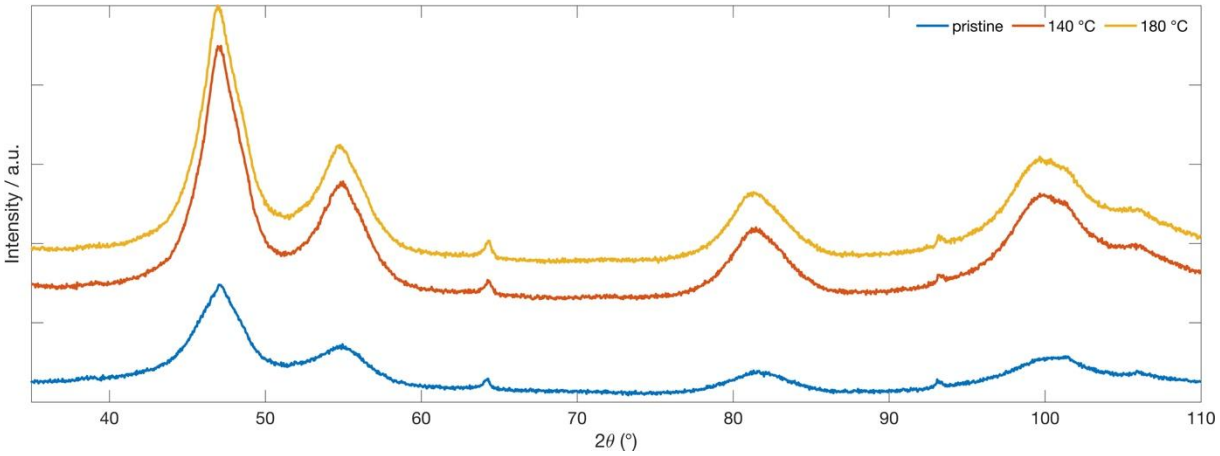

***Figure S3.24**: XRD patterns of Pt-Co/KB, pristine and post-mortem XAS in 95 wt.% H_3PO_4 at various temperature, after ~4 h (specificized in **Table S3.3**), XRD, GDE 1 mg_{metals} cm^{-2}*

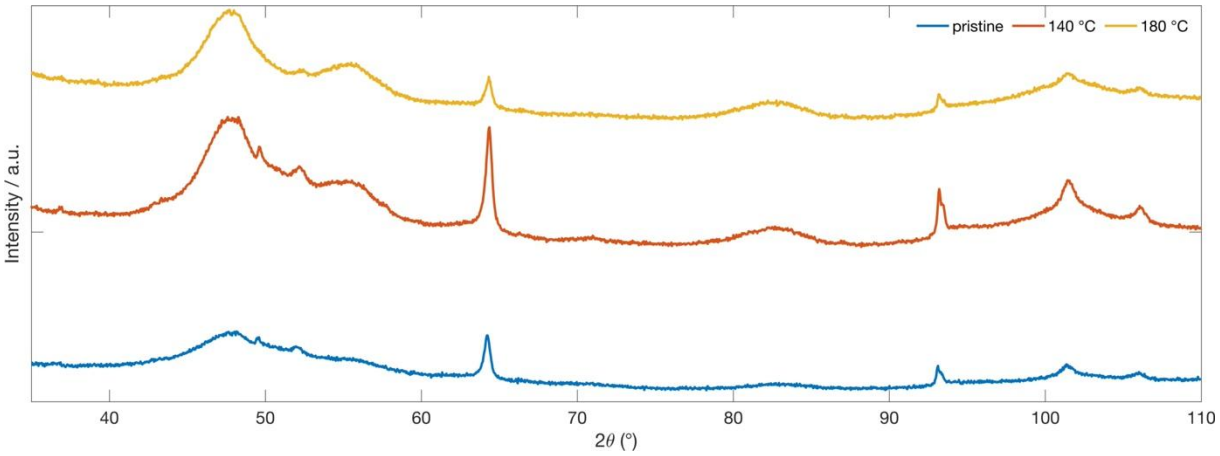

***Figure S3.25**: XRD patterns of Pt-Co/rGO, pristine and post-mortem XAS in 95 wt.% H_3PO_4 at various temperature, after ~ 4 h (specificized in **Table S3.3**), XRD, GDE 1 mg_{metals} cm^{-2}*

4 Activity of the catalysts thin film on RRE in concentrated H_3PO_4 at elevated temperature

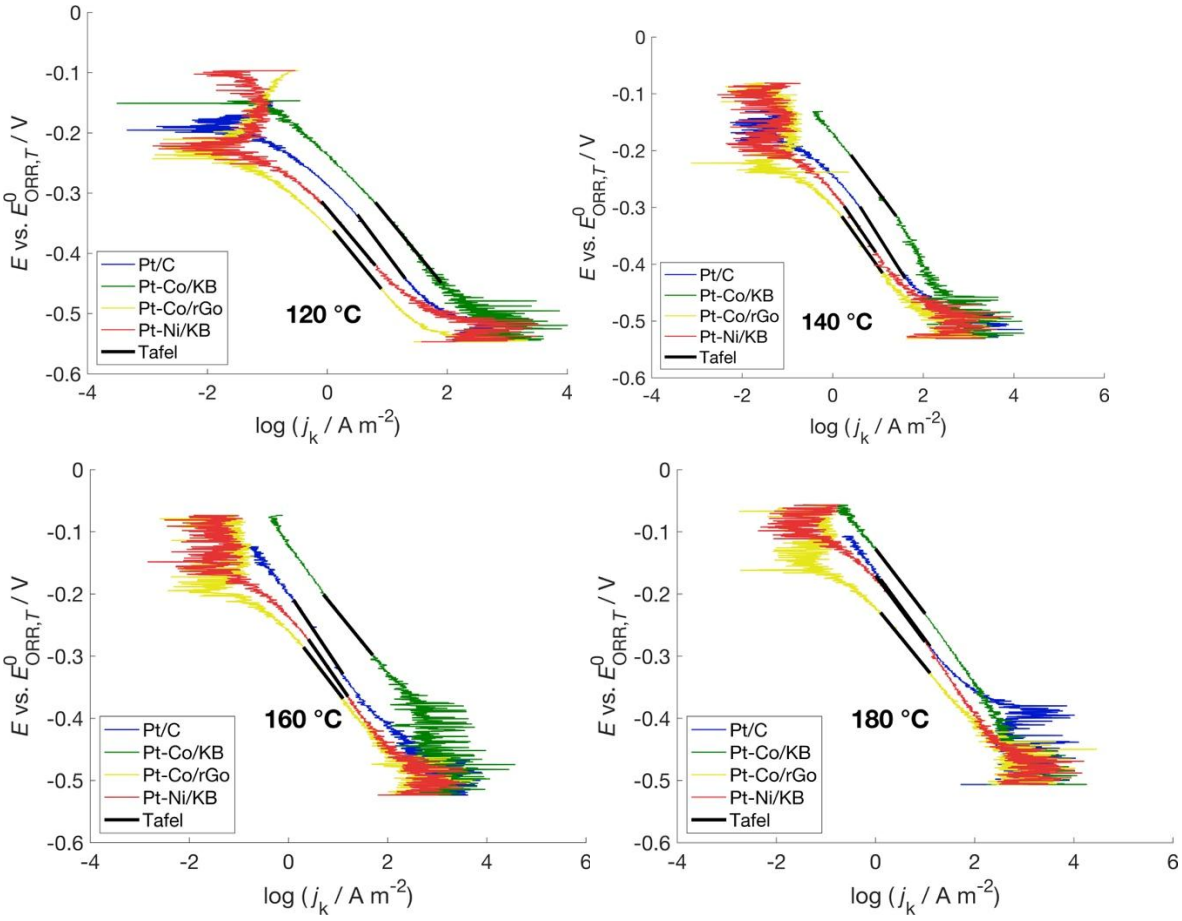

Figure S4.1*: Tafel slope, RRE using revolution rate 2500 rpm; GC electrode, 10 μg_{metals} cm^{-2}, 97.6 wt.% H_3PO_4, 180 °C, 5 mV s^{-1} corrected for background currents and uncompensated resistance, use of corresponding $E_{ORR,g,T}$*

Table S4.1: *Summary of ORR kinetic parameters determined by LSV on RRE using revolution rate 2500 rpm; GC electrode, 10 μg_{metals} cm^{-2}, 97.6 wt.% H_3PO_4, 5 mV s^{-1} corrected for background currents and uncompensated resistance, use of corresponding $E_{ORR,g,T}$, α represents charge transfer coefficient*

Catalyst type	Temperature / °C	j_{ex} / mA m^{-2}	Tafel slope / mV dec^{-1}	α / 1
Pt/C	120	9.6	-133 (R^2 = 0.997)	0.584 ± 0.002
	140	17.7	-127 (R^2 = 0.989)	0.645 ± 0.007
	160	22.4	-120 (R^2 = 0.994)	0.716 ± 0.004
	180	29.3	-108 (R^2 = 0.994)	0.831 ± 0.005
Pt-Co/KB	120	16.1	-122 (R^2 = 0.986)	0.641 ± 0.009
	140	29.7	-108 (R^2 = 0.946)	0.760 ± 0.041
	160	44.6	-98 (R^2 = 0.993)	0.877 ± 0.006
	180	59.7	-104 (R^2 = 0.998)	0.862 ± 0.002
Pt-Co/rGO	120	1.30	-121 (R^2 = 0.996)	0.643 ± 0.003
	140	2.30	-111 (R^2 = 0.972)	0.736 ± 0.021
	160	3.49	-104 (R^2 = 0.987)	0.829 ± 0.011
	180	5.54	-98 (R^2 = 0.998)	0.920 ± 0.002
Pt-Ni/KB	120	1.8	-118 (R^2 = 0.988)	0.658 ± 0.008
	140	4.9	-116 (R^2 = 0.952)	0.703 ± 0.034
	160	10.7	-115 (R^2 = 0.997)	0.746 ± 0.002
	180	25.4	-107 (R^2 = 0.996)	0.841 ± 0.003

Table S4.2: *Activation energy of ORR; methodology according [5] determined by LSV on RRE using revolution rate 2500 rpm, GC electrode, 10 μg_{metals} cm^{-2}, 97.6 wt.% H_3PO_4, 5 mV s^{-1} corrected for background currents and uncompensated resistance, use of corresponding $E_{ORR,g,T}$, c_{O_2} concentration of dissolved oxygen in H_3PO_4 at a given temperature [6-9], H^+ concentration in H_3PO_4 at a given temperature [10, 11] and α charge transfer coefficient from* ***Table S4.1.***

Catalyst type	Use of	$\Delta G^{\ddagger}$ / kJ mol^{-1}
Pt/C	j_{ex}	26.7 ± 1.1 (R^2 = 0.96)
	$\widetilde{k}°_{as}$	16.9 ± 1.9 (R^2 = 0.89)
	$\widetilde{k}°_{dis}$	19.1 ± 1.7 (R^2 = 0.91)
Pt-Co/KB	j_{ex}	32.3 ± 0.5 (R^2 = 0.98)
	$\widetilde{k}°_{as}$	22.2 ± 0.7 (R^2 = 0.97)
	$\widetilde{k}°_{dis}$	25.7 ± 0.6 (R^2 = 0.97)
Pt-Co/rGO	j_{ex}	35.4 ± 0.2 (R^2 = 0.96)
	$\widetilde{k}°_{as}$	24.9 ± 0.2 (R^2 = 0.99)
	$\widetilde{k}°_{dis}$	28.3 ± 0.2 (R^2 = 0.99)
Pt-Ni/KB	j_{ex}	64.8 ± 0.1 (R^2 = 0.99)
	$\widetilde{k}°_{as}$	55.1 ± 0.1 (R^2 = 0.99)
	$\widetilde{k}°_{dis}$	58.6 ± 0.1 (R^2 = 0.99)

5 References

1. Marcano, D.C., et al., *Improved synthesis of graphene oxide.* ACS nano, 2010. **4**(8): p. 4806-4814.
2. Pavko, L., et al., *Toward the continuous production of multigram quantities of highly uniform supported metallic nanoparticles and their application for synthesis of superior intermetallic Pt-Alloy ORR electrocatalysts.* ACS Applied Energy Materials, 2021. **4**(12): p. 13819-13829.
3. Gatalo, M., et al., *A Double-Passivation Water-Based Galvanic Displacement Method for Reproducible Gram-Scale Production of High-Performance Platinum-Alloy Electrocatalysts.* Angewandte Chemie, 2019. **131**(38): p. 13400-13404.
4. Kongkanand, A., *High-Activity Dealloyed Catalysts*. 2014, General Motors LLC, Warren, MI (United States).
5. Buriánek, J., T. Bystron, and K. Bouzek, *Methodology of evaluating the activation energy of oxygen reduction reaction on Pt-based electrodes.* Journal of Electroanalytical Chemistry, 2025: p. 119418.
6. Fleige, M., et al., *Evaluation of temperature and electrolyte concentration dependent Oxygen solubility and diffusivity in phosphoric acid.* Electrochimica Acta, 2016. **209**: p. 399-406.
7. Gan, F. and D.-T. Chin, *Determination of diffusivity and solubility of oxygen in phosphoric acid using a transit time on a rotating ring-disc electrode.* Journal of Applied Electrochemistry, 1993. **23**(5): p. 452-455.
8. Gubbins, K.E. and R. Walker, *Solubility and diffusivity of hydrocarbons and oxygen in fuel cell electrolytes.* Engineering and Industrial Experiment Station, College of Engineering, University of Florida, Contract Number DA-49-186-AMC-45 (X), 1965.
9. Klinedinst, K., et al., *Oxygen solubility and diffusivity in hot concentrated H3PO4.* Journal of Electroanalytical Chemistry and Interfacial Electrochemistry, 1974. **57**(3): p. 281-289.
10. Brown, E.H. and C.D. Whitt, *Vapor pressure of phosphoric acids.* Industrial & Engineering Chemistry, 1952. **44**(3): p. 615-618.
11. Bhardwaj, R., M. Enayetullah, and J.M. Bockris, *Proton activities in concentrated phosphoric and trifluoromethane sulfonic acid at elevated temperature in relation to acid fuel cells.* Journal of the Electrochemical Society, 1990. **137**(7): p. 2070.